Available online at www.sciencedirect.com
ScienceDirect
Journal of Hazardous Materials 155 (2008) 295–304
Journal of Hazardous Materials
www.elsevier.com/locate/jhazmat

Adsorptive removal of the pesticide methomyl using hypercrosslinked polymers

Chiung-Fen Chang [a], Ching-Yuan Chang [b,*], Kuo-En Hsu [b], Shu-Chi Lee [a], Wolfgang Höll [c]

[a] *Department of Environmental Science and Engineering, Tunghai University, Taichung 407, Taiwan*
[b] *Graduate Institute of Environmental Engineering, National Taiwan University, 71 Chou-Shan Road, Taipei 106, Taiwan*
[c] *Forschungszentrum Karlsruhe, Institute for Technical Chemistry, Section WGT, P.O. Box 3640, D-76021 Karlsruhe, Germany*

Received 21 September 2007; received in revised form 16 November 2007; accepted 16 November 2007
Available online 22 November 2007

Abstract

The hypercrosslinked polymers Macronet MN-150 and MN-500 (denoted as MN-150 and MN-500) were investigated to remove the pesticide methomyl from aqueous solutions via adsorption. Furthermore, the effect of humid acid (used as background organic compound) on the adsorption capacity of methomyl for MN-150 was examined. The equilibria and kinetics of the adsorption of methomyl onto MN-150 and MN-500 can be well correlated with Langmuir and Freundlich isotherms, and conventional kinetic models (e.g., surface and pore diffusion models), respectively. The polymer MN-150 possesses a high potential to be applied as adsorbent for the removal of methomyl from aqueous solution when compared with MN-500. Furthermore, the competitive effect of humic acid on adsorption of methomyl on MN-150 can be ignored at low equilibrium concentrations. The transport of methomyl from solution into the polymer adsorbents is controlled by both, external and internal mass transfer mechanisms with film-surface diffusion model offering the better description. The surface mobility and flux of surface diffusion increase as the initial concentration increases.

Keywords: Adsorption; Hypercrosslinked polymer; Methomyl; Equilibrium; Kinetics

1. Introduction

Over the past few decades many processes have been developed and successfully applied for separating substances from the fluid stream and purifying mixtures of substances. Among them, adsorption is commonly recommended as one of the best available control technologies to recover or treat volatile organic compounds from waste streams and drinking water [1]. For water and wastewater treatment, activated carbon (AC) has widely been used to remove contaminants with its well established incomparable record of success as both effective and reliable [2]. Numerous publications on the adsorption of organics on AC have been available in literature in the past [3–9]. The main drawback of AC is the fact that regeneration for re-use is difficult and cost-intensive. Due to high cost of regeneration of the mechanically fragile activated carbons, alternative sorbents such as polymeric resins have been synthesized as potential alternatives to activated carbons.

Macroporous (macroreticular) (co-)polymers of non-ionic polymeric resins are frequently used in water treatment [10]. More recently, hypercrosslinked polymeric adsorbents have been developed which possess widespread applicability because of their large surface area and special functional groups tagged to matrix of polymeric chains. Hypercrosslinked resins are widely used in industries as well as analytical scale [11]. Several reports revealed that hypercrosslinked polymers have high potential for the adsorption of organic [12–16] and inorganic compounds [17], storage of hydrogen [18], etc., interpreting that they were successfully applied in the removal of both organic and inorganic compounds with their unique physical structures.

Pesticides are used worldwide to prevent agriculture from the various kinds of damage, adjust the growth of the plants, and increase the yields of crops. Despite the advantages provided via the usage of pesticides, the residual pesticides remaining in the

* Corresponding author. Tel.: +886 22363 8994; fax: +886 22363 8994.
E-mail address: cychang3@ntu.edu.tw (C.-Y. Chang).

0304-3894/$ – see front matter © 2007 Elsevier B.V. All rights reserved.
doi:10.1016/j.jhazmat.2007.11.057

Nomenclature

a_s	specific external surface area ($m^2\,kg^{-1}$)
A_B	BET surface area ($m^2\,g^{-1}$)
AC	activated carbon
A_L	Langmuir surface area ($m^2\,g^{-1}$)
BDDT	Brunauer, Deming, Deming and Teller
BET	Brunauer, Emmet and Teller
Bi_P	Biot number for the pore diffusion, $k_L\,d_p/(2D_P)$
Bi_S	Biot number for the surface diffusion, $k_L\,d_p\,C_{b0}/(2D_S\,\rho_p\,q_0)$
C	concentration of solute being transferred ($g\,m^{-3}$)
C_b	bulk concentration of solute ($g\,m^{-3}$)
C_{b0}	initial bulk concentration in CSTR ($g\,m^{-3}$)
C_{bI}	surface concentration ($g\,m^{-3}$)
C_e	equilibrium concentration in the liquid phase, q_e ($g\,m^{-3}$)
C_P	adsorbate concentration in the pores at $r = d_P/2$
CSTR	completely stirred tank reactor
d_P	mean particle size (m)
D	diffusivity of the adsorbate in the particles ($m^2\,s^{-1}$)
D_L	liquid molecular diffusivity ($m^2\,s^{-1}$)
D_P	pore diffusion coefficient ($m^2\,s^{-1}$)
D_{Pnh}	theoretical value of D_P under non-hindered diffusion conditions
D_S	surface diffusion coefficient ($m^2\,s^{-1}$)
HPLC	high performance liquid chromatography
IUPAC	International Union of Pure and Applied Chemistry
k_F	Freundlich isotherm constant as specified in Eq. (3) ($(g\,kg^{-1})\,(g\,m^{-3})^{-1/n_F}$)
k_L	external mass transfer coefficient ($m\,s^{-1}$)
K_L	Langmuir isotherm constant as specified in Eq. (2) ($m^3\,g^{-1}$)
m_S	mass of adsorbent (kg)
n_F	Freundlich isotherm constant as specified in Eq. (3)
N_L	mass transfer rate per unit surface area
NOM	natural organic matter
N_P	mass transfer rate per unit of surface area of pore diffusion ($g\,m^{-2}\,s^{-1}$)
N_S	mass transfer rate per unit of surface area of surface diffusion ($g\,m^{-2}\,s^{-1}$)
p, p_0	equilibrium and saturated vapor pressures of adsorbate
q	adsorbate concentration in solid phase ($g\,kg^{-1}$)
q_e	adsorbate concentration in solid phase at equilibrium with C_e ($g\,kg^{-1}$)
q_L	Langmuir isotherm constant as specified in Eq. (2) ($g\,kg^{-1}$)
q_0	q at equilibrium with C_{b0}
r_P	particle radius (m)
r^2	correlation coefficient
R^2	coefficient of determination as specified in Eq. (10)
SAC	strong acid cation
SEM	scanning electron microscopy
STP	standard temperature and pressure
t	Time parameter
T	absolute temperature (K)
TOC	Total organic carbon
V_a	macropore volume ($cm^3\,g^{-1}$)
V_e	mesopore volume ($cm^3\,g^{-1}$)
V_i	micropore volume ($cm^3\,g^{-1}$)
V_L	volume of solution in CSTR (dm^{-3})
V_t	total pore volume ($cm^3\,g^{-1}$)
WBA	weak base anion exchanger
y_c	predicted data as specified in Eq. (10)
y_e	experimental data as specified in Eq. (10)
y_m	average value of the experimental data as specified in Eq. (10)

Greek letters

δ	film thickness (m)
ε_P	adsorbent porosity
ρ_P	apparent particle density ($kg\,m^{-3}$)
ρ_S	particle true density ($kg\,m^{-3}$)
τ	Labyrinth factor or tortuosity of the adsorbent
∇	gradient

environment enhance the latent risk of hazard to the ecosystems and human life. Depending on the chemical composition of pesticides, they exhibit different extents of toxicity for humans and animals. According to European Community Drinking Water Directive, the standards for the individual pesticide and the sum of all pesticides are less than 0.1 and 0.5 $\mu g\,L^{-1}$, respectively, which are both much more stringent than health-based minimum levels set by the World Health Organizations and the US-EPA [19]. In order to meet the stringent pesticide standard of water bodies and protect human health, therefore, it is deemed that remediation technologies of contaminated water are urgently required.

In Taiwan, methomyl is the most commonly used pesticide and takes the top-ranking of aggregate sales among carbamates [20], representing that methomyl possesses high potential threat to environment. Agricultural areas of application are cultivation of vegetables, tobacco, cotton, pasture, soybean, and corn. Some studies on the use of various sorbents for the adsorption of methomyl have been conducted. These sorbents include marine sediments [21], hypercrosslinked poler (HXLGp) [22], and powdered activated carbon [23]. Although the adsorptive removal of methomyl or other pesticides has been examined in previous studies, the application of Macronets MN-150 and MN-500 on the adsorptive removal of methomyl has not been reported. Therefore, the purpose of this study is to examine the adsorptive removal of methomyl by means of using hypercrosslinked polymers. The investigation of adsorption behaviors of methomyl on Macronets included adsorption equilibria and kinetics which are essential for the use in practice. Freundlich and Langmuir

isotherm approaches were used to describe the adsorption equilibrium of methomyl. The conventional kinetic models, such as surface and pore diffusion models, were adopted to simulate the process reaching adsorption equilibrium.

2. Materials and methods

2.1. Adsorbent

Two hypercrosslinked polymers, Macronets MN series (MN-150 and MN-500, supplied by Purolite International Limited, Country offices of Purolite Corporation in Taipei, Taiwan) were used as the adsorbents in this study. Both polymers consist of macroporous polystyrene crosslinked with divinylbenzene, however with different functional groups. MN-150 possesses weakly basic tertiary amine functional groups while MN-500 contains strongly acidic sulphonic acid groups. The physicochemical characteristics of MN-150 and MN-500 were characterized using (1) laser diffraction particle size analyzer (LS 230 with Fluid Volume Module, Beckman Coulter, California, USA) for the representative particle size, (2) Accupyc 1330 (Micromeritics, Georgia, USA) for true density, (3) scanning electron microscopy (SEM, Hitachi S800, Tokyo, Japan) for surface image, and (4) accelerated surface area and porosimetry system (ASAP 2010, Micromeritics, Georgia, USA) for the specific surface area. The pretreatment of the adsorbent comprised three sequential steps: washing with distilled water, drying by centrifuging (CN-2060, Hsiangtai, Taipei, Taiwan) under 5000 rpm for 20 min, and then wetting with distilled water under vacuum, prior to the following adsorption experiments.

2.2. Preparation of methomyl and humic acid solution

A stock solution of methomyl (chemical formula: $C_5H_{10}N_2O_2S$; molecular weight: 162.21) of $1\,g\,L^{-1}$ was prepared by dissolving methomyl (technical material, supplied by TungFong Ltd. Co., Taipei, Taiwan) of 0.2 g in 200 mL of acetonitrile solvent (reagent grade, Merck, Darmstadt, Germany). It was then stored in the teflon-stoppered brown glass bottle. For the subsequent use, the stock solution was diluted to the specific concentrations with ultra-pure water (conductivity of $18\,M\Omega\,cm^{-1}$).

The humic acid salt (technical grade, supplied by Aldrich, Steinheim, Germany) was first dissolved in a solution of $0.1\,mol\,L^{-1}$ NaOH. After complete dissolution, 0.45-μm membrane filter was used to obtain the filtrate. The pH of the filtrate was adjusted to 7 with $0.1\,mol\,L^{-1}$ HCl. The concentration of the humic acid was measured by means of a total organic carbon (TOC) analyzer (Model 1010, O.I. Analytical, Texas, USA). For all experiments, small volumes of a humic acid stock solution ($1000\,g\,m^{-3}$) were added to the methomyl solution. By this means, competitive and high ionic strength effects from the Na Cl content were practically excluded.

2.3. Analytical measurements

For measurements of adsorption equilibrium and kinetic data of the adsorption of methomyl, all samples were filtered through a 0.22 μm membrane filter prior to the analysis, and then measured by means of high performance liquid chromatography (HPLC) with ultra violet (UV) detector (Lab Allence, Pennsylvania, USA). The concentrations were standardized with reagent-grade methomyl (Riedel-de Haën, Seelze, Germany). The wavelength and column used in HPLC were 233 nm and LC-18 (25 cm × 4.6 mm i.d., 5 μm, supplied by Supelco, Inc.), respectively. The volumetric ratio of water to acetonitrile in the solvents is 20/80, in which the solvents compose the eluent for HPLC analysis. Furthermore, the effluent rate was fixed at $1.0\,mL\,min^{-1}$.

2.4. Adsorption equilibrium and kinetics

Experiments for studying adsorption kinetics were conducted in a CSTR. A basket reactor was used in this system to avoid the attrition of adsorbent, which may be encountered in the slurry reactor. The stirring speed was adjusted to 800 rpm in order to ensure the complete mixing and to reduce the film resistance to a minimum. The ratio of adsorbent mass to solution volume was $250\,g\,m^{-3}$ and the temperature was adjusted and controlled at 298 K. Adsorption experiments were stopped after 72 h, i.e., after approximately reaching the adsorption equilibrium (i.e., concentrations of filtrate did not change more than about 3% between two sampling times). In order to investigate the contributive ratios of various mass transfer coefficients, the adsorption experiments were examined at various initial methomyl concentrations (C_{b0}, in the range $<13.8\,g\,m^{-3}$). Furthermore, the equilibrium concentrations (C_e, in the range $<12.4\,g\,m^{-3}$) obtained from various C_{b0} were used to obtain the adsorption isotherm. The amounts of methomyl adsorbed on MN-150 and MN-500 were calculated from the equilibrium concentrations at various C_{b0} to obtain the adsorption isotherm. The specific amount adsorbed in all experiments was calculated from the mass balance:

$$q_e = (C_{b0} - C_e) \times \frac{V_L}{m_S} \quad (1)$$

3. Results and discussion

3.1. Characterization and physicochemical properties of adsorbents

The physicochemical characteristics of MN-150 and MN-500 measured in this study are presented in Table 1. Fig. 1 illustrates the laser diffraction particle size analyses of MN-150 and MN-500. The results show that the median particle sizes of MN-150 and MN-500 are about 662 and 651 μm, respectively. Furthermore, the distribution of particle size is rather uniform for both polymers. Fig. 2 presents the adsorption and desorption isotherms of N_2 at 77 K on MN-150 and MN-500. It can be seen that the adsorption isotherms of MN-150 and MN-500 for the region with adsorbed volumes below or near 250 and $140\,cm^3\,g^{-1}$ STP both belong to type I of the Brunauer, Deming, Deming and Teller (BDDT) classification [24] with well-defined plateaus, indicating that the pores of MN-150 and

Table 1
Physical properties of adsorbents used in the adsorption experiments

Property	MN-150	MN-500
Average particle size[a], d_P (mm)	0.662	0.651
Specific external surface area[b], a_S ($m^2\,kg^{-1}$)	13	9.6
Particle true density[c], ρ_S ($kg\,m^{-3}$)	1187	1318
Apparent particle density[d], ρ_P ($kg\,m^{-3}$)	697	960
Particle porosity[e], ε_P	0.41	0.27
Surface area[f] ($m^2\,g^{-1}$)		
Langmuir, A_L	1187	423
BET, A_B	822	414
Micropore area[g] ($m^2\,g^{-1}$)	564	296
Pore volume ($cm^3\,g^{-1}$)		
Total, V_t	0.592	0.283
Micro-, V_i	0.261	0.137
Meso-[h], V_e	0.180	0.092
Macro-[h], V_a	0.151	0.054
Average pore diameter[i] (Å)	29	27

[a] Analyzed using LS 230 Fluid Module.
[b] Assumed as sphere and calculated using $a_s = 6/(\rho_P \times d_P)$.
[c] Analyzed using Accupyc 1330, Micromeritics.
[d] Calculated using $1/((1/\rho_S) + V_t)$. V_t = total pore volume per unit mass of adsorbent.
[e] Calculated using $1 - (\rho_P/\rho_S)$.
[f] Analyzed using ASAP2010, Micromeritics.
[g] Calculated using t-method.
[h] Calculated using $V_t - V_i = V_e + V_a$, with Barrett, Joyner and Hanlenda (BJH) adsorption pore distribution, which gives the proportions of mesopore to macropore volumes.
[i] Calculated using $4V_t/A_B$.

MN-500 are microporous. Concurrently, when the relative pressure (p/p_0) is close to 1, the adsorbed volumes for both polymers abruptly increase, indicating that both polymers possess mesoporous structures because the developments are well fitting to the type II of the BDDT classification. These results are entirely consistent with the pore volumes as shown in Table 1.

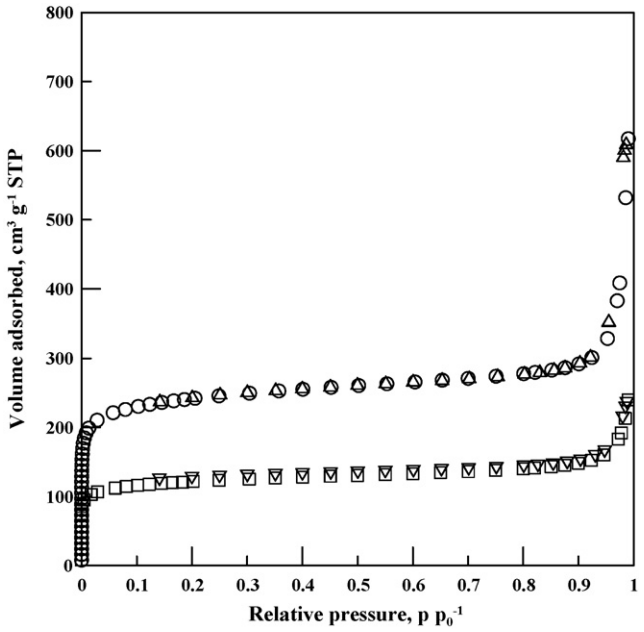

Fig. 2. Adsorption (◯) and (□), and desorption (△) and (▽) isotherms of N_2 at 77 K on adsorbents: (◯) and (△), and (□) and (▽): experimental data of MN-150 and MN-500, respectively.

The Brunauer, Emmet and Teller (BET) specific surface area of MN-150 amounts to 822 $m^2\,g^{-1}$, which is in the range of the commercial activated carbon, F-400 (Filtrasorb 400, Chemviron, European Operation of Calgon Carbon Corporation), which is 1026 $m^2\,g^{-1}$ [25]. Furthermore, the micro-porous area of 564 $m^2\,g^{-1}$ and the average pore diameter of 29 Å also reflect that MN-150 is a highly potential adsorbent. The data determined in this study are in accordance with those given by Purolite Corporation. Compared to MN-150, MN-500 possesses a smaller BET specific surface area (i.e., 414 $m^2\,g^{-1}$). With this resin there is a significant difference to the data provided by Purolite Corporation (i.e., 800–1000 $m^2\,g^{-1}$). For hypercrosslinked polymers, the specific surface area actually

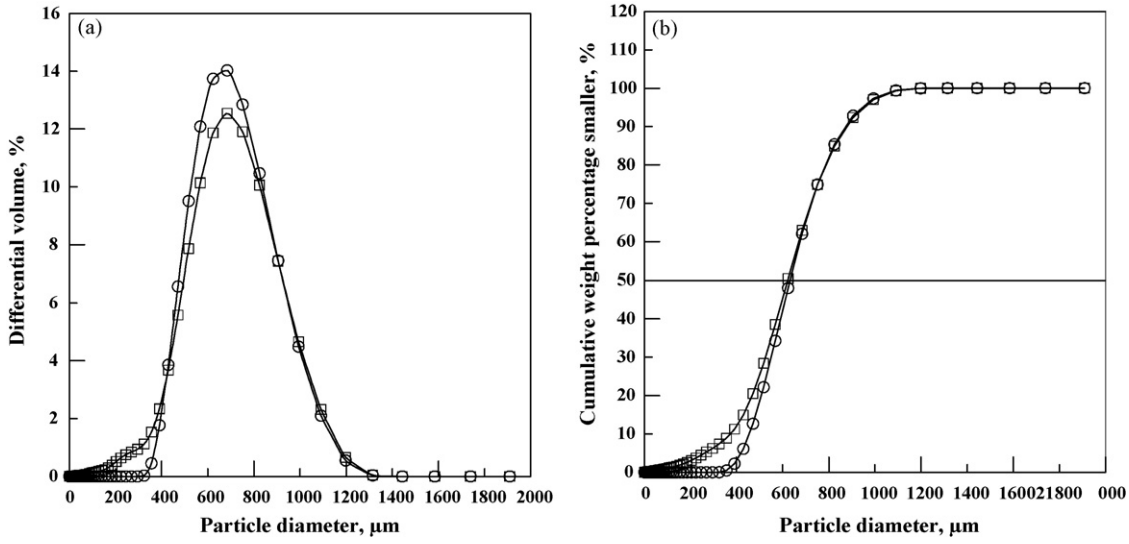

Fig. 1. The relationship between the particle diameter, differential volume (a) and accumulated mass percentage (b): (◯) and (□) experimental data of MN-150 and MN-500, respectively.

represents the surface area associated with voids between the crosslinked poly-chains rather than with the pores between the walls [11]. As opposed to the traditional adsorbents such as activated carbon and zeolite, hypercrosslinked polymer possesses swelling phenomena resulting from the contact with nitrogen during the measurement. Therefore, the porous structure of hypercrosslinked polymers is flexible, which causes the difficulty of parameter estimation and inaccuracy of the pore structure and surface area. Nevertheless, the pores structure is likely explained by the hysteresis loop of adsorption–desorption curves. The hysteresis loops of MN-150 and MN-500 with nearly parallel branches resemble type H4 of International Union of Pure and Applied Chemistry (IUPAC) classification [26], which manifests the existence of slit-shaped pores for both polymers.

Photographs of the surfaces of MN-150 and MN-500 are presented in Fig. 3. The shapes of MN-150 and MN-500 are essentially spherical as shown in Fig. 3a. Along with the increase of the amplification factor, SEM pictures display much more rough and irregular surface structures of both, MN-150 and MN-500, as can be seen in Fig. 3b. The SEM image shows that the pore structures of MN-150 and MN-500 are due to the crosslinks

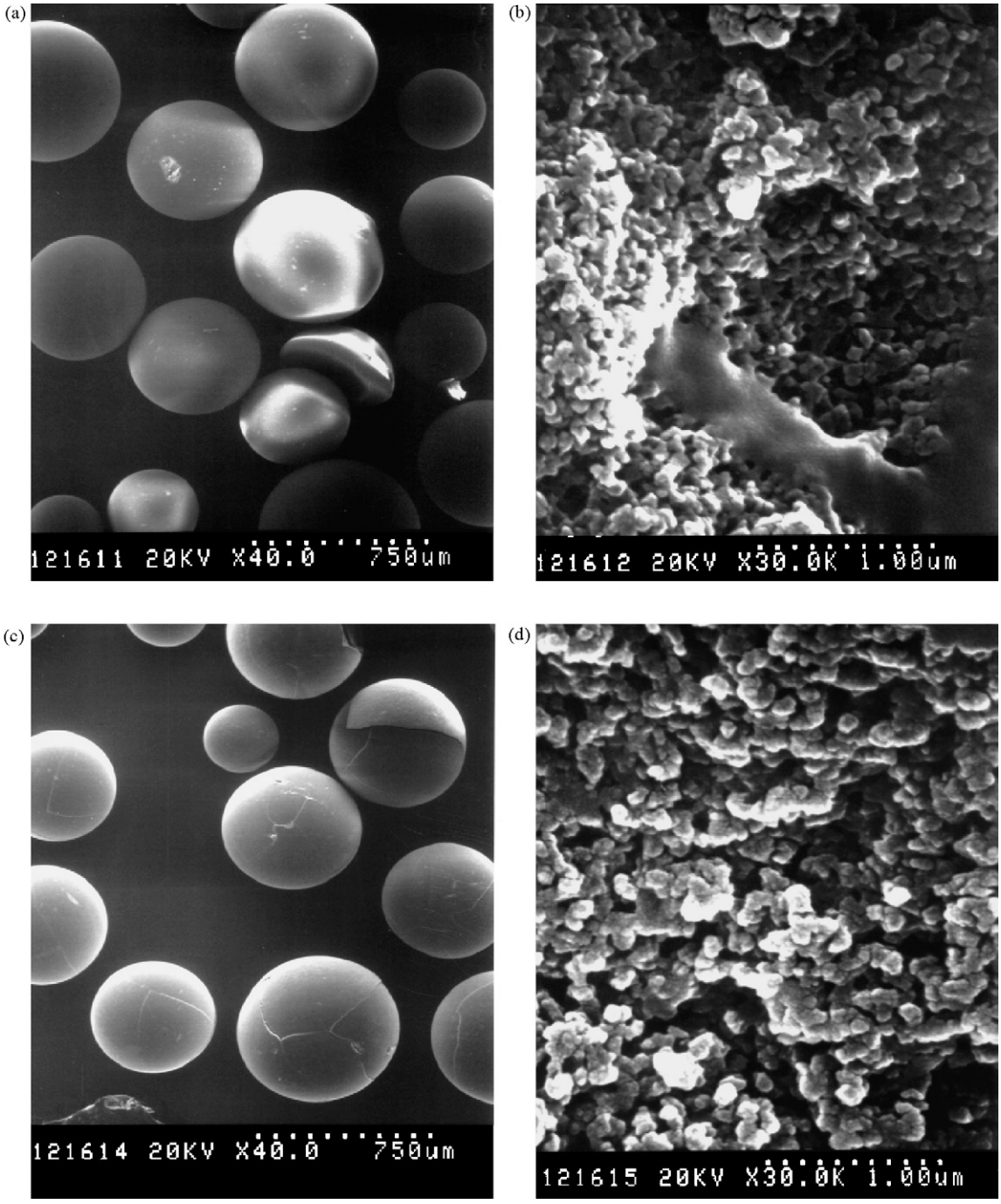

Fig. 3. SEM pictures of Macronet MN-150 and MN-500. Top: MN-150; bottom: MN-500.

of polymeric matrices and both polymers are homogeneous single-phase materials.

3.2. Adsorption equilibrium

The chemical name of methomyl is S-methyl *N*-(methylcarbamoyloxy) thioacetimidate and the molecular weight is 162. According to the physicochemical properties of methomyl investigated in previous study [27], methomyl is quite stable in the pH range of 2–8. However, at a pH value greater than 10, methomyl becomes unstable and degradable. Approximately 12 and 0%, respectively, of the original concentrations still remain at pH values of 10 and 12. In order to simulate the natural environment, the pH value investigated in this study is neutral.

Langmuir and Freundlich equations were used to describe the adsorption isotherm data of methomyl with their widely good applicabilities in water treatment. The mathematical formulas of Langmuir and Freundlich isotherms are given in Eqs. (2) and (3), respectively:

$$q_e = \frac{q_L K_L C_e}{1 + K_L C_e} \tag{2}$$

$$q_e = k_F C_e^{\,1/n_F} \tag{3}$$

In Eq. (2), q_L and K_L are the Langmuir isotherm constants, of which the former expresses the monomolecular coverage of the surface of adsorbent, while the latter stands for equilibrium constant. In Eq. (3), k_F and n_F are the Freundlich equilibrium constants, which represent the adsorption capacity and strength of adsorption, respectively.

The constants of both adsorption isotherms can be determined from the adsorption isotherm data by means of following equations:

$$\frac{C_e}{q_e} = \frac{1}{q_L K_L} + \frac{C_e}{q_L} \tag{4}$$

$$\frac{1}{q_e} = \left(\frac{1}{q_L K_L}\right)\frac{1}{C_e} + \frac{1}{q_L} \tag{5}$$

$$\ln q_e = \frac{1}{n_F}\ln C_e + \ln k_F \tag{6}$$

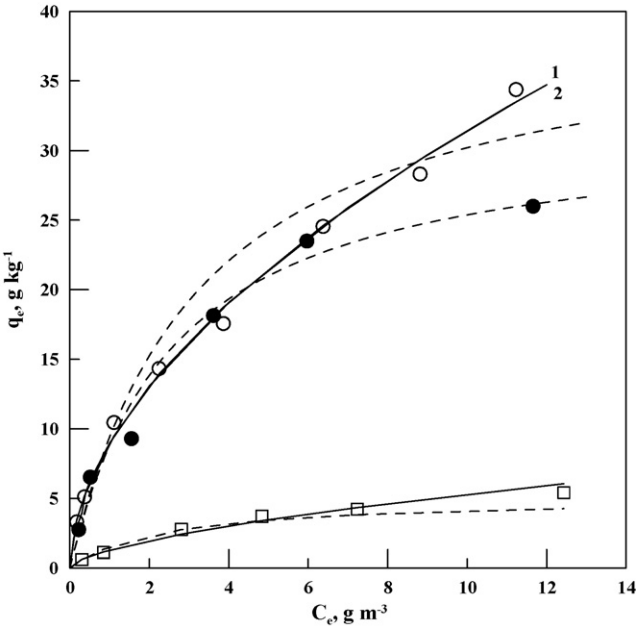

Fig. 4. Correlation of experimental data by means of the Freundlich (—) and Langmuir isotherms (- - -) for the adsorption of methomyl: (◯) MN-150, (□) MN-500 (single component systems) and (●) MN-150 in mixed system with humic acid (C_{b0} of 3 g m^{-3}). Lines 1 and 2 are the Freundlich isotherms for adsorption of methomyl in single solute systems and mixed systems on MN150.

Eqs. (4) and (5) were used for MN-150 and MN-500, respectively. The selection of the linearising form of the Langmuir isotherm depends on the emphasis on data in either low or high equilibrium concentrations. The plot of $1/C_e$ versus $1/q_e$ or C_e versus C_e/q_e is able to calculate the constants K_L and q_L from the slope of straight line and intercept. The n_F and k_F values can be obtained from the plot of $\ln q_e$ versus $\ln C_e$ via the same calculation procedure for the Langmuir isotherm constants. The results are shown in Table 2 and Fig. 4. The values of q_L and K_L for the adsorptions of methomyl on MN-150, and MN-500 are 24 and 5 g kg^{-1} (q_L), and 0.89 and 0.43 m^3 g^{-1} (K_L), respectively. The results indicate that MN-150 possesses a larger adsorption capacity for methomy than MN-500. The values of n_F of the Freundlich isotherms show that MN-150 and MN-500 allow a favorable uptake of methomyl from the

Table 2
Values of adsorption isotherm parameters and correlation coefficients (r^2)[a] of adsorptions of methomyl on MN-150 and MN-500

System	Langmuir isotherm			Freundlich isotherm		
	q_L (g kg^{-1})	K_L (m^3 g^{-1})	$r_L^{2,b}$	k_F ((g kg^{-1}) (g m^{-3})$^{-1/n_F}$)	n_F	$r_F^{2,b}$
MN-150[c,d]						
Single solute of methomyl	40	0.31	0.9334	8.97	1.84	0.996
Bisolutes of methomyl and humic acid[f]	32	0.43	0.9789	7.59	1.83	0.964
MN-500[c,e]	5.07	0.43	0.9828	1.29	1.63	0.988

[a] The units for C_e and q_e are g m^{-3} and g kg^{-1}, respectively.
[b] r_L^2 and r_F^2 are correlation coefficients by means of fitting the experimental data to Langmuir and Freundlich isotherms, respectively.
[c] The range of the equilibrium concentrations of the experiments performed is 0–12.4 g m^{-3} for MN-150 and MN-500.
[d] The linearising equation adopting Eq. (4).
[e] The linearising equation adopting Eq. (5).
[f] The initial concentration of humic acid is 3 g m^{-3}.

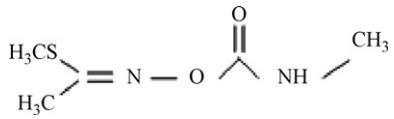

Fig. 5. Structure of methomyl.

aqueous solution. Furthermore, the correlation coefficients (i.e., $r_L{}^2$ and $r_F{}^2$ are both greater than 0.96) revealing that both Langmuir and Freundlich isotherms can well describe the equilibrium of the adsorption of methomyl onto MN-150 and MN-500 in the whole experimental range.

The structure of methomyl is illustrated in Fig. 5, which shows several lone-pair electrons pairs on nitrogen, oxygen, and sulfur atoms. Furthermore, the adsorption of methomyl on polymers is attributed to the dispersion forces and polarization of π-electrons (electron-rich part of the adsorbate). For the sulphonic acid functional groups tagged to the structure of MN-500, the repulsion force between lone-pair electrons of methomyl and sulphonate ($R–SO_2O^-$) of the polymer may significantly reduce the adsorption capacity for methomyl. The tertiary amine functionality of MN-150 possesses a positive charge on nitrogen atom, which may contribute the attraction force with lone-pair electrons of methomyl, leading to the high adsorption capacity of methomyl on MN-150.

Natural organic matter (NOM) is ubiquitous in the environment and mainly comprises compounds of humic acid, fulvic acid and other humic substances. With NOM in the system, the adsorption capacity for target compounds is usually reduced [15,28]. The effect of NOM on the adsorption capacity of methomyl on polymer MN-150 was also investigated in this study, as shown in Table 2 and Fig. 4. The results indicate that the presence of humic acid, of which the initial concentration was 3 g m^{-3}, affected the adsorption of methomyl in the low concentration range (i.e., equilibrium concentrations <6 g m^{-3}) only slightly, but obviously reduced the adsorption capacity in the high concentration range (i.e., at equilibrium concentration of 11.7 g m^{-3}). Comparison of the values of q_L of methomyl as a single solute on MN-150 and of systems with methomyl and humic acid, the monolayer adsorption capacity of methomyl decreased due to the competitive adsorption of humic acid. However, the adsorption strength of methomyl, judged from the value of n_F essentially remains the same, which may demonstrate the greater affinity of methomyl for MN-150. As a consequence of the results it can be stated that the presence of humic acid does not influence the adsorption of methomyl onto MN-150 when the equilibrium concentration is below 6 g m^{-3}.

3.3. Adsorption kinetics

The traditional models of adsorption kinetics usually encompass a complicated mathematical computation to obtain the respective mass transfer and diffusion coefficients of the models, such as external and internal mass transfer coefficients [29,30]. For the sake of determination of related coefficients, the external mass transfer coefficients were computed first. In the further calculations, the internal diffusion coefficients were determined combined with the external mass transfer coefficients calculated in the first step.

3.3.1. External mass transfer

The external mass transfer coefficient (k_L) is derived from Ficks' First Law, as shown in the following equation:

$$N_L = -D_L \nabla C = -k_L(C_b - C_{bI}) \quad (7)$$

$k_L(=D_L/\delta)$ predominantly depends on the hydrodynamic flow across the surface of the adsorbent particles and other factors that may affect the molecular diffusivity of fluid or liquid (D_L) and film thickness (δ), such as the viscosity of the solvent and temperature. In order to reduce or eliminate the film mass transfer resistance in the CSTR experiments, the stirring speed is kept at a high speed of 800 rpm. At the very beginning of the experimental time, it can be assumed that adsorption is exclusively controlled by the external mass transfer so that the surface concentration (C_{bI}) is zero or at negligible level when compared to the bulk concentration (C_b). From the assumptions mentioned above, k_L can be calculated by means of Eq. (8) [31]:

$$\ln \frac{C_b}{C_{b0}}\bigg|_{t\to 0} = -k_L \frac{m_S a_S}{V_L} t, \quad \text{with } a_s = \frac{6}{\rho_P d_P} \quad (8)$$

The values of k_L obtained from various experimental conditions are shown in Table 3. For both adsorbents the k_L values decrease with increasing initial concentration (C_{b0}), which can be interpreted as greater mass transfer resistance at higher initial

Table 3
Transport quantities of methomyl on MN-150 and MN-500 in the aqueous system

Adsorbent	C_{b0} (g m^{-3})	Film mass transfer coefficient	Internal diffusion coefficients						
			Surface diffusion			Pore diffusion			
		k_L (m s^{-1})	D_S (m^2 s^{-1})	R^2	Bi_S	D_P (m^2 s^{-1})	R^2	D_{Pnh}	N_s/N_P
MN-150	1.0	4.0×10^{-5}	5.9×10^{-14}	0.956	36	5.6×10^{-10}	0.965	1.1×10^{-10}	3.99
	1.7	3.5×10^{-5}	7.1×10^{-14}	0.965	33	4.1×10^{-10}	0.980	1.1×10^{-10}	2.65
	6.0	1.7×10^{-5}	7.1×10^{-14}	0.989	29	2.2×10^{-10}	0.990	1.1×10^{-10}	0.96
	8.3	1.3×10^{-5}	7.2×10^{-14}	0.968	26	1.7×10^{-10}	0.989	1.1×10^{-10}	0.51
MN-500	1.1	9.0×10^{-6}	8.7×10^{-14}	0.987	28	1.1×10^{-10}	0.995	4.9×10^{-11}	1.26
	3.5	7.2×10^{-6}	1.1×10^{-13}	0.965	28	9.0×10^{-11}	0.990	4.9×10^{-11}	0.85
	5.8	3.6×10^{-6}	1.2×10^{-13}	0.977	16	7.5×10^{-11}	0.970	4.9×10^{-11}	0.54
	8.3	2.1×10^{-6}	1.7×10^{-13}	0.968	7	5.0×10^{-11}	0.990	4.9×10^{-11}	0.03

concentrations. Comparison of the values of k_L of MN-150 and MN-500 at the similar C_{b0} indicates that the film mass transfer of methomyl is faster in the case of MN-150, of which the reason may be that the attraction between methomyl and MN-150 promotes the transfer rate, while the adsorption rate of methomyl on the surface of MN-500 may be reduced due to the less effective collision of the methomyl molecule resulted from electrostatic repulsion.

3.3.2. Internal mass transfer

The internal mass transfer of methomyl on polymer adsorbents was investigated by means of using surface diffusion and pore diffusion models in this study. The governing equations of the coupled surface diffusion and pore diffusion models are Eqs. (9) and (10), respectively. A more detailed discussion of these equations is adequately given in Refs. [31–34].

$$\left(\frac{\varepsilon_P}{\rho_P}\right)\frac{\partial C_P}{\partial t} + \frac{\partial q}{\partial t} = D_S\left(\frac{\partial^2 q}{\partial r^2} + \frac{2}{r}\frac{\partial q}{\partial r}\right) \tag{9}$$

$$\varepsilon_P\frac{\partial C_P}{\partial t} + \rho_P\frac{\partial q}{\partial t} = D_P\left(\frac{\partial^2 C_P}{\partial r^2} + \frac{2}{r}\frac{\partial C_P}{\partial r}\right) \tag{10}$$

Both equations have to be solved for the respective initial and boundary conditions. Combination with external mass transfer results from the boundary condition at the surface of the particles. The respective mass balance equation for the transfer of methomyl from the liquid to solid phases (i.e., external film transfer) can be described as follows [31]:

$$N_L = -k_L(C_b - C_{bI}) = -D\frac{\partial C_P}{\partial r}, \quad \text{at } r = \frac{d_P}{2} \tag{11}$$

The applicability of model on intraparticle kinetics of methomyl can be judged by the coefficient of determination (R^2), as follows:

$$R^2 = 1 - \frac{\sum(y_e - y_c)^2}{\sum(y_e - y_m)^2} \tag{12}$$

The results of simulation with surface and pore diffusion are shown in Table 3 and Fig. 6.

Both models satisfactorily fitted the data of the CSTR experiments with high accuracy (i.e., high value of coefficient of determination). Thus, either the combined film/surface or film/pore diffusion model is able to describe the development of adsorption within the time range of the experiments quite well. The surface diffusion coefficient D_S generally increases with increasing C_{b0}, while the pore coefficient D_P decreases with increasing C_{b0}. Furthermore, with increasing C_{b0}, the values of D_S for both adsorbents appear to approach constant values of about 7×10^{-14} and 1.7×10^{-13} m^2 s^{-1}, respectively, within the experimental range. The apparently or really increasing mobility of methomyl on MN-150 and MN-500 may be attributed to the occupation of sites with weaker binding energy at high concentrations. The decrease of D_P values can be attributed to the contribution of surface diffusion, which will be discussed further in the next paragraph. For further discussion of the predominant mass transfer resistance for the transport of methomyl from the aqueous to the solid phase, the Biot number for the surface diffusion, Bi_S ($=k_L d_p C_{b0}/2D_s\rho_P q_0$), has been examined to judge the relative influence of the external and internal diffusion mass transfer resistances. Table 3 shows that the values of Bi_S for both MN-150 and MN-500 systems are smaller than 50 while greater than 1. This leads to the conclusion that the mass transfer of methomyl on the adsorbents is controlled by both film and surface diffusion.

The value of D_P can theoretically be estimated under the assumption of non-hindered diffusion, as shown in Eq. (13)

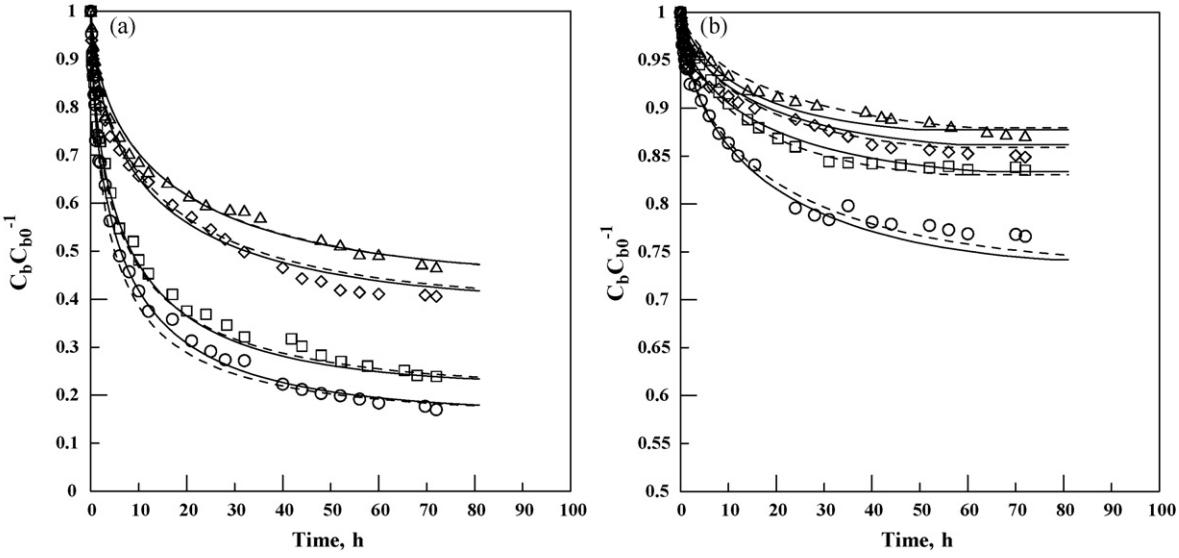

Fig. 6. C_b/C_{b0} vs. adsorption time for adsorption of methomyl on Macronet MN adorbents at stirring speed of 800 rpm and temperature of 298 K in CSTR system. C_{b0} and C_b: concentrations of methomyl at $t = 0$ and t. (△), (◇), (□) and (◯): $C_{b0} = 1.0$, 1.7, 6.0, and 8.3 g m^{-3} for MN-150, and $C_{b0} = 1.1$, 3.5, 5.8, and 8.3 g m^{-3} for MN-500. (—) and (- - -): simulation prediction using surface diffusion model and pore diffusion model, respectively. (a) MN-150 and (b) MN-500.

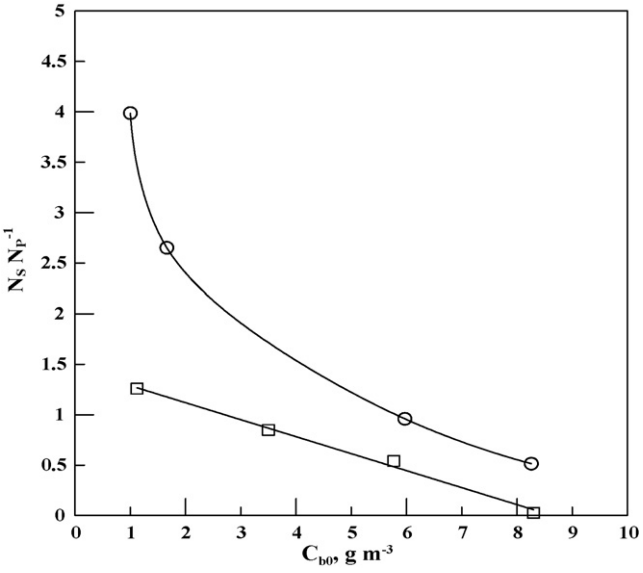

Fig. 7. Relationship between the flux ratio of surface diffusion to pore diffusion and initial concentration C_{b0}. (◯) and (□): data of MN-150 and MN-500, respectively.

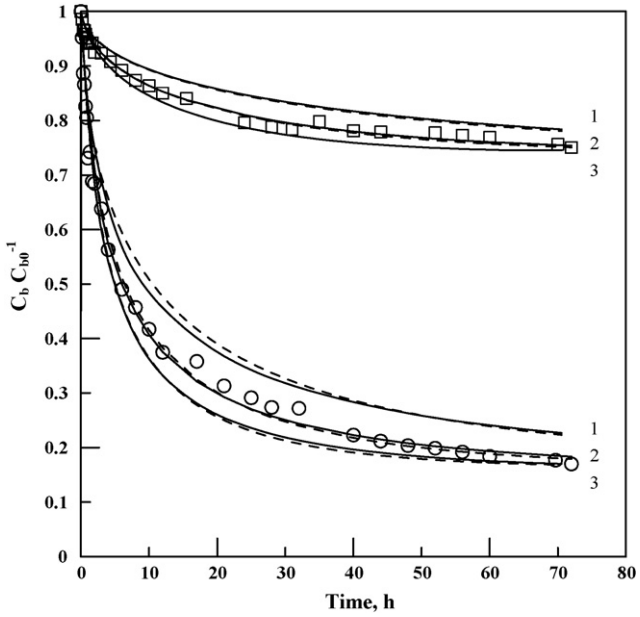

Fig. 8. Comparison of C_b/C_{b0} predicted by surface and pore models with experimental data of adsorption kinetics at stirred speed of 800 rpm in CSTR. (◯) and (□): experimental data of MN-150 and MN-500. (—) and (- - -): fitted by means of surface diffusion and pore diffusion models, respectively. Groups 1–3: data calculated by 50% of D_S and D_P (i.e., $D_S0.5$ and $D_P0.5$), 100% of D_S and D_P (i.e., D_S and D_P), and 150% of D_S and D_P (i.e., $D_S1.5$ and $D_P1.5$), respectively. $C_{b0} = 1\ g\ m^{-3}$.

[31,35]:

$$D_{Pnh} = \frac{\varepsilon_P D_L}{\tau} \quad \text{with } \tau = {\varepsilon_P}^{-1} \tag{13}$$

Prior to the determination of D_{Pnh}, the liquid molecular diffusivity D_L of methomyl has been calculated by means of the Wilke-Chang correlation [36] leading to a value of $6.7 \times 10^{-10}\ m^2\ s^{-1}$. The difference between D_{Pnh} and D_P gradually reduces with increasing C_{b0} for the adsorbents MN-150 and MN-500. The most likely explanation for the reason with D_p greater than D_{Pnh} is that the D_p calculated from the fitting of experimental data is an effective diffusion coefficient obtained with consideration of the flux of surface diffusion. An estimation of the ratio of the surface to pore diffusion mass transport under the assumption of combined diffusion can be obtained from [31]:

$$\frac{N_S}{N_P} = \frac{\tau}{\varepsilon_P D_L}\left[D_P - \frac{D_L \varepsilon_P}{\tau}\right] \tag{14}$$

where N_S and N_P are the mass transfer rates per unit of surface area ($g\ m^{-2}\ s^{-1}$) of surface diffusion and pore diffusion, respectively. The results of the respective calculations are illustrated in Table 3 and Fig. 7.

For both polymers the mass flux ratio of surface to pore diffusion decreases as the initial concentration C_{b0} increases. Thus pore diffusion plays as significant a role as surface diffusion. This indicates a system with weak interactions between adsorbent and solute. As a consequence, pore diffusion dominates the intraparticle diffusion at high C_{b0}, which is sufficiently supported by noting that the value of D_P approaches to that of D_{Pnh} at high C_{b0}. Furthermore, the Biot number for the pore diffusion, Bi_P ($=k_L d_p/2D_p$), is examined to evaluate the relative influence of the external and internal pore mass transfer resistances. E.g., with MN-500 and at $C_{b0} = 8.3\ g\ m^{-3}$, the value of Bi_P is about 14, representing that the use of the film-pore diffusion model is also able to properly describe the mass transfer of methomyl. In addition, the internal diffusion coefficients obtained at $C_{b0} = 1\ g\ m^{-3}$ with both, MN-150 and MN-500, are taken as examples to investigate the sensitivity of the model, as shown in Fig. 8. Combinations of values of 50 and 150% of D_S and D_P (i.e., $D_{S0.5}$, $D_{S1.5}$, $D_{P0.5}$ and $D_{P1.5}$) are used to predict the development of concentration in the CSTR. Comparing the results with D_S, D_P, $D_{S0.5}$, $D_{S1.5}$, $D_{P0.5}$ and $D_{P1.5}$, the obvious deviation of the predicted values is found in the transition range between the rapid and slow adsorption zones. Higher internal diffusion coefficients (e.g., $D_{S1.5}$ and $D_{P1.5}$) enhance the adsorption rate and reduce the equilibration time.

4. Conclusions

The equilibrium and kinetics of the adsorption of methomyl on the hypercrosslinked polymers Macronet MN-150 and MN-500 were investigated in this study. The results demonstrate that MN-150 possesses promising properties to be used as adsorbent for removal of methomyl from aqueous solutions. The equilibrium of adsorption onto the two adsorbents can well be described by either the Freundlich or Langmuir isotherm relationships. The small adsorption capacity of methomyl on MN-500 may be attributed to repulsive forces between sulphonic acid functional groups and lone-pair electrons of methomyl. The presence of humid acid as background organic compound in the solution does not affect the adsorption capacity of methomyl on MN-150 at small equilibrium concentrations. The kinetics of adsorption of methomyl on MN-150 and MN-500 can be described by the

film-surface diffusion model. The surface mobility and flux of surface diffusion increase with the increasing initial concentration.

Acknowledgments

The authors thank for the National Science Council of Taiwan for the financial support under Grant NSC 94-2211-E-002-018 and NSC 95-2221-E-002-019, and the Powder Technology Laboratory of Chemical Engineering Department of National Taiwan University for the assistance in powder characterization.

References

[1] M.J. Ruhl, Recover VOCs via adsorption on activated carbon, Chem. Eng. Prog. 89 (7) (1993) 37–41.
[2] C. Tien, Adsorption Calculations and Modeling, Butterworth–Heinemann Series in Chemical Engineering, Boston, MA, USA, 1994.
[3] C.F. Chang, C.Y. Chang, W.T. Tsai, Adsorption equilibrium of polyethylene glycol in the copper electroplating solution on activated carbon, J. Colloid Interface Sci. 232 (2) (2000) 207–209.
[4] C.F. Chang, C.Y. Chang, K.H. Chen, W.T. Tsai, J.L. Shie, Y.H. Chen, Adsorption of naphthalene on zeolite from aqueous solution, J. Colloid Interface Sci. 266 (2) (2003) 273–279.
[5] C.F. Chang, C.Y. Chang, W. Höll, Investigating the adsorption of 2-mercaptothiazoline on activated carbon from aqueous system, J. Colloid Interface Sci. 272 (1) (2004) 52–58.
[6] C.Y. Chang, W.T. Tsai, C.H. Ing, C.F. Chang, Adsorption of polyethylene glycol (PEG) from aqueous solution onto hydrophobic zeolite, J. Colloid Interface Sci. 277 (1) (2004) 29–34.
[7] W. Den, H.C. Liu, S.F. Chan, K.T. Kin, C.P. Huang, Adsorption of phthalate esters with multiwalled carbon nanotubes and its application, J. Environ. Eng. Manage. (formerly J. Chin. Inst. Environ. Eng.) 16 (4) (2006) 275–282.
[8] P.E. Diaz-Flores, R. Leyva-Romos, J.R. Rangel-Mendez, M.M. Ortiz, R.M. Guerrero-Coronado, J. Mendoza-Barron, Adsorption of 2,4-dichlorophenoxyacetic acid from aqueous solution on activated carbon cloth, J. Environ. Eng. Manage. (formerly J. Chin. Inst. Environ. Eng.) 16 (4) (2006) 249–257.
[9] G.S. Wang, Effects of natural organic matter on adsorption capacity for atrazine by activated carbon, J. Chin. Inst. Environ. Eng. 15 (1) (2005) 81–89.
[10] M.P. Tsyurupa, L.A. Maslova, A.I. Andreeva, T.A. Mrachkovskaya, V.A. Davankov, Sorption of organic compounds from aqueous media by hypercrosslinked polystyrene sorbents 'Styrosorb', React. Polym. 25 (1) (1995) 69–78.
[11] M.P. Tsyurupa, V.A. Davankov, Porous structure of hypercrosslinked polystyrene: state-of-the-art mini-review, React. Funct. Polym. 66 (7) (2006) 68–779.
[12] M. Streat, L.A. Sweetland, Physical and adsorptive properties of Hypersol-Macronet^{TM} polymers, React. Funct. Polym 35 (1–2) (1997) 99–109.
[13] M. Streat, L.A. Sweetland, Removal of pesticides from water using hypercrosslinked polymer phases. Part 1. Physical and chemical characterization of adsorbents, Process Saf. Environ. Protect.: Trans. Inst. Chem. Eng. 76 (B2) (1998) 115–126.
[14] M. Streat, L.A. Sweetland, Removal of pesticides from water using hypercrosslinked polymer phases. Part 2. Sorption studies, Process Saf. Environ. Protect.: Trans. Inst. Chem. Eng. 76 (B2) (1998) 127–134.
[15] M. Streat, L.A. Sweetland, Removal of pesticides from water using hypercrosslinked polymer phases. Part 3. Mini-column studies and the effect of fulvic and humic substances, Process Saf. Environ. Protect.: Trans. Inst. Chem. Eng. 76 (B2) (1998) 135–141.
[16] M. Streat, L.A. Sweetland, Removal of pesticides from water using hypercrosslinked polymer phases. Part 4. Regeneration of spent adsorbents, Process Saf. Environ. Protect.: Trans. Inst. Chem. Eng. 76 (B2) (1998) 142–150.
[17] B. Saha, M. Streat, Adsorption of trace heavy metals: application of surface complexation theory to a macroporous polymer and a weakly acidic ion-exchange resin, Ind. Eng. Chem. Res. 44 (23) (2005) 8671–8681.
[18] P.M. Budd, M. Peter, A. Butler, The potential of organic polymer-based hydrogen storage materials, Phys. Chem. Chem. Phys. 9 (15) (2007) 1802–1808.
[19] Drinking Water Directive (DWD) of European Community, Council Directive 98/83/EC, July 2007. http://www.ec.europa.eu/environment/water/water-drink/index_en.html.
[20] COAT (Council of Agriculture of Taiwan), July 2006. http://www.bulletin.coa.gov.tw/index_intro.php.
[21] G.P. Yang, Y.H. Zhao, X.L. Lu, X.C. Gao, Adsorption of methomyl on marine sediments, Colloid Surf. A: Physicochem. Eng. Aspects 264 (1–3) (2005) 179–186.
[22] N. Fontanals, M. Galia, P.A.G. Cormack, R.M. Marce, D.C. Sherrington, F. Borrull, Evaluation of a new hypercrosslinked polymer as a sorbent for solid-phase extraction of polar compounds, J. Chromatogr. A 1075 (1–2) (2005) 51–56.
[23] J.Y. Hu, T. Aizawa, Y. Magara, Evaluation of adsorbability of pesticides in water on powdered activated carbon using octanol–water partition coefficient, Water Sci. Technol. 35 (7) (1997) 219–226.
[24] S. Braunauer, L.S. Deming, W.S. Deming, E. Teller, On a theory of the van der Waals adsorption of gases, J. Am. Chem. Soc. 62 (7) (1940) 1723–1732.
[25] C.F. Chang, C.Y. Chang, W.T. Tsai, Effects of burn-off and activation temperature on preparation of activated carbon from corn cob agrowaste by CO_2 and steam, J. Colloid Interface Sci. 232 (1) (2000) 45–49.
[26] S. Lowell, J.E. Shields, Powder Surface Area and Porosity, 3rd ed., Chapman & Hall, NY, USA, 1991.
[27] C.F. Chang, C.Y. Chang, K.E. Hsu, W. Höll, P.C. Chiang, Removal of pesticide of methomyl by adsorption using novel hypercrosslinked polymer of Marcronet MN-100, J. Environ. Eng. Manage. (formerly J. Chin. Inst. Environ. Eng.) 17 (15) (2007) 311–318.
[28] F.H. Frimmel, M. Assenmacher, M. Sorensen, G. Abbt-Braun, G. Grabe, Removal of hydrophilic pollutants from water with organic adsorption polymers. Part 1. Adsorption behaviour of selected model compounds, Chem. Eng. Process 38 (4) (1999) 601–610.
[29] C.F. Chang, C.Y. Chang, W. Hoell, Adsorption behavior of 2-naphthalenesulfonate on activated carbon from aqueous systems, Ind. Eng. Chem. Res. 42 (26) (2003) 6904–6910.
[30] E.L. Cussler, Diffusion: Mass Transfer in Fluid Systems, Cambridge University Press, NY, USA, 1997.
[31] H. Sontheimer, J.C. Crittenden, R.S. Summers, Activated Carbon for Water Treatment, DVGW-Forschungsstelle, Karlsruhe, Germany, 1998.
[32] R.G. Peel, A. Benedek, Dual rate kinetic model of fixed bed adsorber, J. Environ. Eng. Div. 106 (4) (1980) 797–813.
[33] R.G. Peel, A. Benedek, C.M. Crowe, A branched pore kinetic model for activated carbon adsorption, AIChE J. 27 (1) (1981) 26–32.
[34] C.F. Chang, C.Y. Chang, W. Höll, M. Ulmer, Y.H. Chen, H.J. Groß, Adsorption kinetics of polyethylene glycol from aqueous solution onto activated carbon, Water Res. 38 (10) (2004) 2559–2570.
[35] M. Suzuki, Adsorption Engineering, Kodansha, Tokyo, Japan, 1990.
[36] C.R. Wilke, P. Chang, Correlation of diffusion coefficients in dilute solutions, AIChE J. 1 (2) (1955) 264–270.